

Full paper

Visible-light-driven overall water splitting with a largely-enhanced efficiency over a Cu₂O@ZnCr-layered double hydroxide photocatalyst



Chong Wang^a, Bin Ma^b, Simin Xu^a, Dapeng Li^a, Shan He^a, Yufei Zhao^c, Jingbin Han^{a,*},
Min Wei^{a,*}, David G. Evans^a, Xue Duan^a

^a State Key Laboratory of Chemical Resource Engineering, Beijing Advanced Innovation Center for Soft Matter Science and Engineering, Beijing University of Chemical Technology, Beijing 100029, PR China

^b Université Grenoble Alpes, ISTERre, F-38058 Grenoble, France

^c Key Laboratory of Photochemical Conversion and Optoelectronic Materials, Technical Institute of Physics and Chemistry Chinese Academy of Sciences, Beijing 100190, PR China

ARTICLE INFO

Keywords:

Overall water splitting
Layered double hydroxides
Electron-hole transportation
Interface modification

ABSTRACT

Overall water splitting through solar radiation is highly attractive for alternative energy utilization. Herein, we designed and fabricated a Cu₂O@ZnCr-layered double hydroxide (LDH) core-shell photocatalyst to achieve a high-performance, visible-light overall water splitting. The Cu₂O@ZnCr-LDH nanostructure exhibits a high activity (with H₂ and O₂ production rate of 0.90 and 0.44 μmol h⁻¹, respectively) under visible-light without any sacrificial agent and co-catalyst, which is among the highest level of reported photocatalysts under the same conditions. Both experimental and computational investigations demonstrate that the Cu₂O@ZnCr-LDH heterostructure fully exploits the synergistic effect of Cu₂O and ZnCr-LDH, in terms of band structure matching. Most significantly, the S₂O₃²⁻ group in the gallery of ZnCr-LDH acts as an effective mediator between these two individual components, which not only inhibits the photocorrosion of Cu₂O but also accelerates the immigration of photo-induced electron-hole pairs. Therefore, this work provides a deep insight for the design and preparation of visible-light-responsive photocatalysts, which show promising applications in photochemical reactions and energy conversion.

1. Introduction

Photocatalytic overall water splitting *via* solar energy and semiconductor photocatalysts provides an effective strategy to explore green and sustainable energy [1]. Since the initiative work by Fujishima and Honda on water splitting by TiO₂ [2], various photocatalysts including transition metal (Fe, Co, Ni, Mo Sn and W) oxides and derivative compounds (nitrides, borides, phosphides, sulfides and carbides) have been explored as promising candidates [3–10]. Admittedly, in the design of semiconductor photocatalysts, both an enhanced light utilization and prompted separation/transportation of photogenerated electron-hole pair are extremely important to fully utilize the photo-response of materials [11–16]. Although great efforts have been made to improve these two key factors, the efficiency of overall water splitting is still not satisfied because of limited visible-light response and undesirable electron-hole recombination arising from random charge flow [17–20]. Therefore, how to achieve highly-efficient, visible-light-induced photocatalysts by virtue of material design and synthesis exploration remains a big challenge.

Cu₂O, as a well-known p-type semiconductor, has a narrow band gap (~2.0 eV), which exhibits a high photochemical activity toward water splitting under visible light [21]. However, the disproportionation reaction of Cu⁺ into Cu²⁺ and Cu⁰ induces a serious photocorrosion, which restricts its practical application as high-efficiency photocatalyst [22]. Therefore, to enhance the stability of Cu₂O and maintain its photochemical activity simultaneously is a conundrum. A variety of methods have been employed to improve the photocatalytic performance of Cu₂O, for instance, *via* suitable textural design, doping or fabricating a heterojunction with another semiconductor/metal [23–26]. These approaches, to some extent, push forward the exploitation of Cu₂O-based photocatalysts for visible-light water splitting, but the poor photostability and facile electron-hole recombination still remain unsolved.

Layered double hydroxides (LDHs) is a class of laminar materials generally expressed as [M_{1-x}^{II}M_x^{III}(OH)₂](Aⁿ⁻)^{x/n}·mH₂O (M^{II} and M^{III} are divalent and trivalent metals respectively, Aⁿ⁻ is interlayer anion for charge balance) [27,28]. Some transition-metal-bearing LDH materials (*e.g.*, ZnCr-, NiTi- and CoFe-LDHs) have shown semicon-

* Corresponding authors.

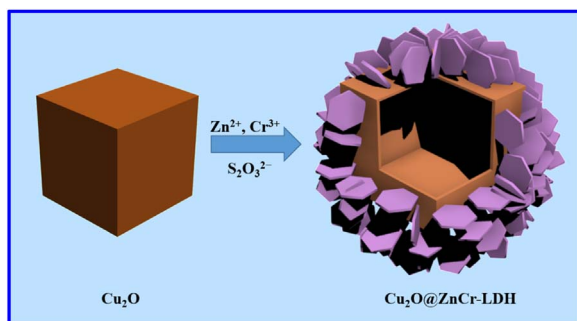
E-mail addresses: hanjb@mail.buct.edu.cn (J. Han), weimin@mail.buct.edu.cn (M. Wei).

<http://dx.doi.org/10.1016/j.nanoen.2017.01.010>

Received 14 November 2016; Received in revised form 4 January 2017; Accepted 5 January 2017

Available online 06 January 2017

2211-2855/ © 2017 Elsevier Ltd. All rights reserved.



Scheme 1. Schematic illustration for the preparation of $\text{Cu}_2\text{O}@/\text{ZnCr-LDH}$ hollow core-shell photocatalyst.

ductor behaviour in degradation of pollutants and photocatalytic oxygen evolution reaction [29–32]. Nevertheless, the photocatalytic overall water splitting over these materials has rarely been reported because of their high recombination rate of photoexcited electron-hole. If LDHs material is integrated with another band-structure-matched semiconductor to produce a Z-scheme heterojunction, a fine control over the directed charge flow of electrons and holes can be achieved; this would improve the utilization efficiency of photogenerated carriers and the resulting H_2/O_2 production. Furthermore, the interfacial property of the heterojunction can be modulated by the interlayer anion of LDHs, so as to accelerate the transportation of photoexcited electron-hole at the heterojunction interface. Based on this design diagram, an optimization of photocatalytic performance toward visible-light-induced overall water splitting should be expected.

In this work, a $\text{Cu}_2\text{O}@/\text{ZnCr-LDH}$ core-shell photocatalyst was obtained by fabricating ZnCr-LDH nanoplates on hollow Cu_2O nanocubes *via* an *in situ* crystallization-selective etching method (Scheme 1), which exhibits extremely high overall water splitting capability under visible light without any sacrificial agent and co-catalyst. During the formation of $\text{Cu}_2\text{O}@/\text{ZnCr-LDH}$ core-shell structure, the interlayer anion $\text{S}_2\text{O}_3^{2-}$ in ZnCr-LDH plays a crucial role for the interfacial optimization by the formation of a chemical bonding $\text{Cu}-(\text{S}_2\text{O}_3^{2-})/\text{LDH}$, which is confirmed by X-ray photoelectron spectroscopy (XPS) and extended X-ray absorption fine structure (EXAFS). This leads to a strong interfacial interaction between these two semiconductors and guarantees a high structural integrity of Z-scheme heterojunction, which is rather superior to previously reported composite photocatalysts. Most significantly, both the experimental and calculational studies substantiate that the presence of $\text{Cu}-(\text{S}_2\text{O}_3^{2-})/\text{LDH}$ bond facilitates the separation and transportation of photogenerated electron-hole at the heterojunction interface, which results in a high efficiency for the utilization of photoexcited carriers and hence largely improved H_2/O_2 production.

2. Experimental section

2.1. Synthesis of Cu_2O nanocubes

Cu_2O nanocubes were synthesized using a similar method with previously reported work [33]. The detailed synthesis process is shown in the Supporting Information.

2.2. Synthesis of $\text{Cu}_2\text{O}@/\text{ZnCr-LDH}$ nanospheres

The $\text{Cu}_2\text{O}@/\text{ZnCr-LDH}$ nanospheres were prepared by using Cu_2O nanocubes as soft template according to Pearson's hard and soft acid-base (HSAB) principle [34]. An *in situ* crystallization of ZnCr-LDH nanoplates shell on the surface of Cu_2O nanocubes was carried out by the following procedure: 100 mg of freshly prepared Cu_2O was dispersed into deionized water (100 ml); then ZnCl_2 (50 mg, ~ 0.4 mmol) and $\text{CrCl}_3 \cdot 6\text{H}_2\text{O}$ (50 mg, ~ 0.2 mmol) were dissolved in

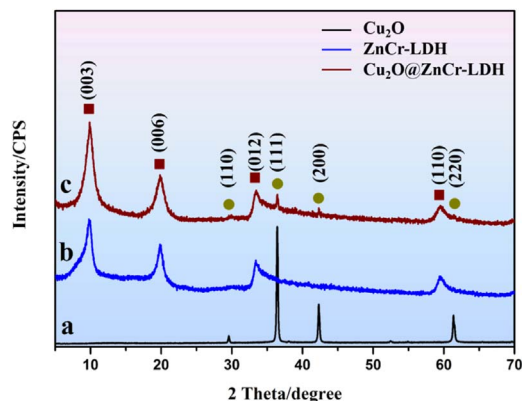


Fig. 1. XRD patterns of (a) Cu_2O , (b) ZnCr-LDH and (c) $\text{Cu}_2\text{O}@/\text{ZnCr-LDH}$ sample.

this solution under magnetic stirring. Afterwards, $\text{Na}_2\text{S}_2\text{O}_3$ solution (1 mol/L, 20 ml) was dropped into the above solution with stirring at room temperature for a fixed period. Finally, the resulting $\text{Cu}_2\text{O}@/\text{ZnCr-LDH}$ core-shell nanospheres were washed thoroughly with water and anhydrous ethanol, and dried under freeze-drying for 12 h. As a control sample, the pure ZnCr-LDH nanoplate powdered sample was prepared by a hydrothermal method [35].

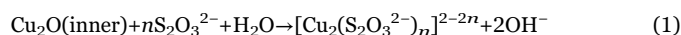
The sample characterization, calculation details on band structure over various samples, and photocatalytic evaluation toward visible-light-driven overall water splitting are described in the Supporting Information.

3. Results and discussion

3.1. Structural and morphological characterizations

Fig. 1 shows the XRD patterns of resulting $\text{Cu}_2\text{O}@/\text{ZnCr-LDH}$ nanospheres, with pristine Cu_2O and ZnCr-LDH as reference samples. The typical diffraction peaks at 29.55° , 36.35° , 42.28° and 61.34° are indexed to the (110), (111), (200) and (220) reflection of a Cu_2O phase (PDF # 65–3288) (curve a). For ZnCr-LDH (curve b), the peaks at 10.05° , 19.90° , 33.36° and 59.60° are attributed to the (003), (006), (012) and (110) reflection of ZnCr-LDH phase. The interlayer space (d_{003}) is calculated to be ~ 0.879 nm, indicating the intercalation of $\text{S}_2\text{O}_3^{2-}$ ions in the gallery of ZnCr-LDH. In the case of $\text{Cu}_2\text{O}@/\text{ZnCr-LDH}$ sample, a superimposed pattern of Cu_2O and LDH phase is observed (curve c), which demonstrates the integration of these two compositions with fine crystallization and high purity. Moreover, the formation of $\text{Cu}_2\text{O}@/\text{ZnCr-LDH}$ structure with $\text{S}_2\text{O}_3^{2-}$ in the interlayer region of ZnCr-LDH was confirmed by FT-IR measurement (see details in the Supporting Information, Fig. S1).

The morphology of $\text{Cu}_2\text{O}@/\text{ZnCr-LDH}$ was investigated by SEM and HR-TEM observations. Fig. 2A shows a typical SEM image of pristine Cu_2O , which possesses well-dispersed cubic shape with mean particle size of ~ 200 nm. During the *in situ* growth process of ZnCr-LDH with Cu_2O as template, numerous intercrossing nanoplates with a vertical orientation are observed on the surface of Cu_2O core (Fig. 2B–D). HR-TEM images (Fig. 2E–H) reveal that the Cu_2O core was inwards etched to produce a cavity structure with exposed (100) facet, resulting in the flower-like, hollow $\text{Cu}_2\text{O}@/\text{ZnCr-LDH}$ with a core-shell architecture. In addition, the core-shell architecture is further verified by EDS analysis (Fig. S2), from which it is observed that both Zn and Cr are homogeneously distributed throughout the outer shell and Cu is located in the core of nanosphere. The formation mechanism of $\text{Cu}_2\text{O}@/\text{ZnCr-LDH}$ could be explained by the HSAB principle and Kirkendall effect *via* the coordination effect between cuprous ion and thiosulfate [36,37], as described in the following reactions:



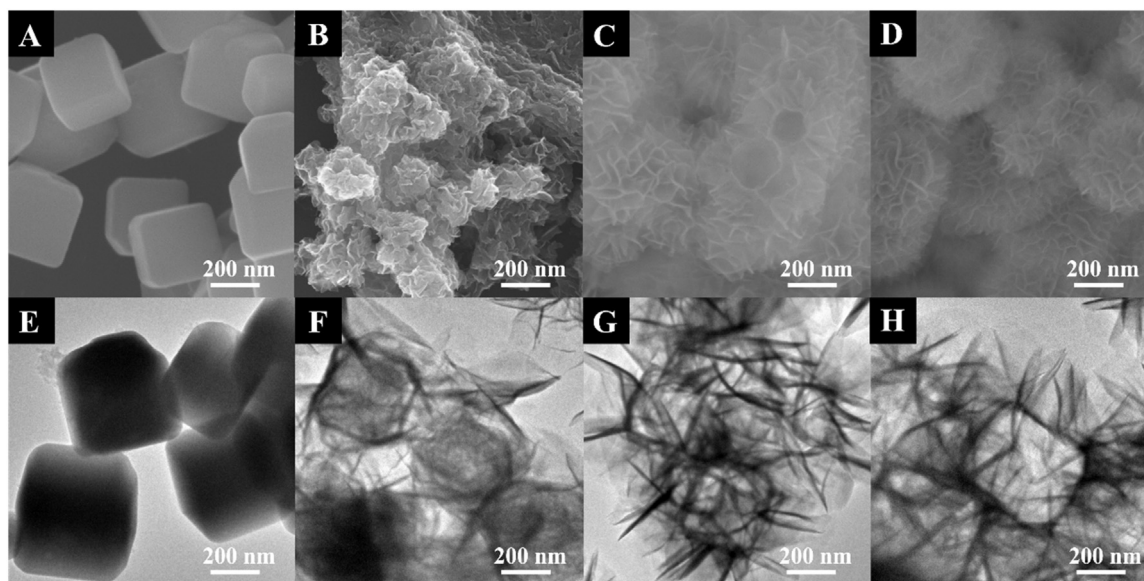
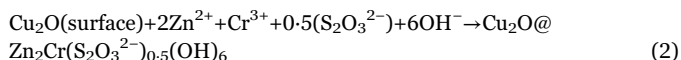


Fig. 2. (A–D) SEM and (E–H) HR-TEM images of $\text{Cu}_2\text{O}@ZnCr\text{-LDH}$ nanospheres synthesized with different reaction time (from left to right): 0 min, 10 min, 30 min and 60 min, respectively.



Ionized Cu^+ as soft acid are prone to react with the soft base $\text{S}_2\text{O}_3^{2-}$ to form soluble $[\text{Cu}_2(\text{S}_2\text{O}_3^{2-})_n]^{2-2n}$ and OH^- , resulting in an inwards etching of cubic Cu_2O . Simultaneously, a co-precipitation reaction of Zn^{2+} and Cr^{3+} occurs under alkaline conditions to produce ZnCr-LDH nanoplate on the surface of Cu_2O ; $\text{S}_2\text{O}_3^{2-}$ anions enter into the gallery region of ZnCr-LDH laminate to maintain the charge balance. By this preparation route, hollow $\text{Cu}_2\text{O}@ZnCr\text{-LDH}$ nanospheres with a thin-layer Cu_2O core and LDH nanoplates shell are obtained. This growth mechanism will be further discussed in the next section. The incomplete etching of Cu_2O is confirmed by ion-conductive plasma (ICP) measurements, which shows a decrease in the mass fraction of Cu element from 20% to 6% (Fig. S3) with an extension of reaction time from 10 to 60 min.

In addition to the $\text{Cu}_2\text{O}@LDH$ system with Zn^{2+} and Cr^{3+} in the LDH slab, the constitute of LDH shell can be exchanged by other metal elements, including Co^{2+} , Ni^{2+} and Ga^{3+} . A series of core-shell structure, for instance, $\text{Cu}_2\text{O}@CoNi\text{-LDH}$, $\text{Cu}_2\text{O}@NiGa\text{-LDH}$ and $\text{Cu}_2\text{O}@NiCr\text{-LDH}$ were also successfully synthesized by using the same strategy. XRD patterns (Fig. S4) of these samples show superimposition of individual Cu_2O and LDH reflection, indicating successful hybridization of the two components. SEM images (Fig. S5) further verify the growth of various LDH shell on the Cu_2O surface, resulting in flower-like nanospheres with the similar morphology as $\text{Cu}_2\text{O}@ZnCr\text{-LDH}$ sample. This demonstrates the versatility of template-assisted strategy for the preparation of tunable $\text{Cu}_2\text{O}@LDH$ materials with potential applications.

3.2. Studies on electronic and coordination structure of $\text{Cu}_2\text{O}@ZnCr\text{-LDH}$

The UV–Vis diffuse reflection spectrum (DRS) was carried out to investigate the photoresponse property of the $\text{Cu}_2\text{O}@ZnCr\text{-LDH}$ nanosphere. As shown in Fig. 3A, Cu_2O sample exhibits a weak and broad peak in the range 400–800 nm assigned to the Cu–O–Cu bond. ZnCr-LDH exhibits two strong bands at ~ 410 nm and ~ 570 nm, which are attributed to the ligand-to-metal charge-transfer effect from 2p orbital of O to 3d orbital of Cr^{3+} and from Cr 3d_{tg} orbital to Cr 3d_{eg} orbital, respectively [38]. After hybridization with Cu_2O , the peak at ~ 570 nm undergoes an obvious blue shift, indicating a strong interaction

between Cu_2O core and ZnCr-LDH shell. Notably, the intensity of the two absorption bands for $\text{Cu}_2\text{O}@ZnCr\text{-LDH}$ nanospheres is stronger than those of ZnCr-LDH , demonstrating a further enhanced photo-response property of $\text{Cu}_2\text{O}@ZnCr\text{-LDH}$.

Photoluminescence (PL) spectrum is an effective tool to study the recombination of free carriers in photocatalysts. Cu_2O sample shows no obvious PL emission peak; pure ZnCr-LDH displays a strong emission at ~ 470 nm (Fig. 3B) due to the withdrawing of photoexcited electrons back to the ground state. An obvious decrease in PL intensity is observed for the $\text{Cu}_2\text{O}@ZnCr\text{-LDH}$ sample in comparison with pristine ZnCr-LDH , which confirms a largely enhanced electron-hole separation/transport rather than recombination at the ground state. This probably arises from the band structure matching between Cu_2O and ZnCr-LDH , which promotes the transport efficiency of carriers.

Fine-scan X-ray photoelectron spectroscopy (XPS) was used to gain a better understanding of the electronic structure of $\text{Cu}_2\text{O}@ZnCr\text{-LDH}$. The XPS survey spectrum of $\text{Cu}_2\text{O}@ZnCr\text{-LDH}$ (Fig. S6A) reveals the presence of Zn, Cr, Cu, O and S element, in good agreement with EDS result. The binding energies of pristine ZnCr-LDH at 1046.2 and 1023.1 eV correspond to Zn 2p_{1/2} and Zn 2p_{3/2}, respectively (Fig. S6B). For the $\text{Cu}_2\text{O}@ZnCr\text{-LDH}$ nanospheres, however, these two energies shift to 1045.8 and 1022.6 eV, respectively. Concomitantly, the peaks of Cr 2p_{1/2} and Cr 2p_{3/2} for $\text{Cu}_2\text{O}@ZnCr\text{-LDH}$ nanospheres exhibit a similar shift to low energy (Fig. S6C). The decreased binding energies of Zn and Cr 2p orbitals indicate an electron transfer from Cu_2O core to LDH shell. For the Cu element, the binding energies of 2p_{1/2} and 2p_{3/2} undergo a 0.3 and 0.4 eV positive shift relative to pristine Cu_2O , respectively (Fig. S6D), which is attributed to the partial oxidation of Cu_2O at the interface. Meanwhile, for the S element (Fig. S6E), the peaks located at ~ 162.2 and ~ 168.0 eV are ascribed to the 2p binding energy of Cu–S bond and interlayer $\text{S}_2\text{O}_3^{2-}$ anion, respectively. The electronic coupling effect between Cu_2O and LDH may accelerate the electron-hole separation process, which will be discussed in the next section.

Extended X-ray absorption fine structure (EXAFS) spectroscopy was further applied to give an investigation on coordination characteristics of the $\text{Cu}_2\text{O}@ZnCr\text{-LDH}$ sample. The Cu K-edge EXAFS spectrum of $\text{Cu}_2\text{O}@ZnCr\text{-LDH}$ is shown in Fig. 4A, with Cu foil, Cu_2O and CuO as reference samples. Two pre-edge peaks appear at 8.984 and 8.992 keV, which are ascribed to the dipole-allowed 1s→4p electron transition for Cu (I) and Cu (II), respectively, indicative of two

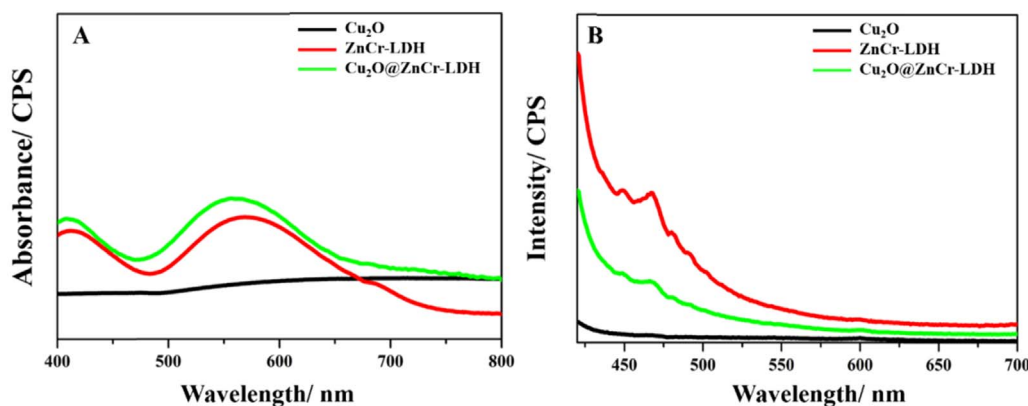


Fig. 3. (A) UV-Vis diffuse reflection spectra (DRS) and (B) photoluminescence (PL) spectra of: Cu₂O, ZnCr-LDH and Cu₂O@ZnCr-LDH.

oxidation states of Cu element [39]. For the Cu₂O@ZnCr-LDH sample, the pre-edge peak energy is located between Cu₂O and CuO, indicating that the oxidation state of copper is between +1 and +2, but rather close to +1. The local order of the coordination environment around copper atoms is expressed by the oscillations from 2.5 to 12 Å⁻¹ in the k^3 -weighted EXAFS (Fig. 4B). Upon Fourier transform (FT) of the EXAFS oscillations, two characteristic peaks at $R + \Delta R = 1.5$ Å and 3.09 Å are observed for Cu₂O sample (Fig. 4C), which are attributed to its first shell of Cu–O bond and the higher shell of Cu–Cu bond, respectively [40]. In the case of Cu₂O@ZnCr-LDH sample, the first shell of Cu–O bond exhibits a positive shift of ~ 0.2 Å after the formation of heterostructure, which can be fitted with the Cu–O and Cu–S backscattering pairs at $R = 1.95$ Å and 2.22 Å (Table 1), respectively. In contrast, the Cu–Cu peak at $R + \Delta R = 3.09$ Å shows a decreased intensity without obvious shift after incorporating with ZnCr-LDH, indicating a significant decrease in the coordination number (CN) of Cu–Cu in Cu₂O@ZnCr-LDH sample compared with Cu₂O reference. Actually, the fitting results of EXAFS (Table 1) demonstrate that the CN of Cu–Cu decreases from ~ 12.0 (Cu₂O) to ~ 2.6 (Cu₂O@ZnCr-LDH), which can be attributed to inner etching of Cu₂O nanocubes during the synthesis of Cu₂O@ZnCr-LDH. In addition, the CN of Cu–O decreases from ~ 1.9 (Cu₂O) to ~ 1.0 (Cu₂O@ZnCr-LDH), accompanied with the presence of Cu–S bond with CN of ~ 1.5 from the fitting analysis of EXAFS (Table 1). These results indicate the formation of chemical bonding of Cu–(S₂O₃²⁻)/LDH at the heterostructure interface. In such structure, S₂O₃²⁻ interacts with positively-charged LDH matrix *via*

electrostatic force; the chemical bonding decreases the electron density of Cu⁺ and induces a valence state larger than +1, in accordance with the location of pre-peak. Based on the XPS and EXAFS results, the Cu₂O core in Cu₂O@ZnCr-LDH heterostructure includes two parts, *i.e.* the inner part is Cu–O component and the outer surface is modified by Cu–S bond (as schematically illustrated in Fig. 4D).

3.3. Photocatalytic performance

The photocatalytic performance toward water splitting over different samples was evaluated by monitoring the time dependent production of H₂ and O₂ under visible light ($\lambda > 400$ nm) without any sacrificial agent and co-catalyst. As shown in Fig. 5, the ZnCr-LDH nanoplates do not show any activity for water splitting under the visible light. Although Cu₂O nanocubes display a H₂ and O₂ generation rate of 0.32 and 0.14 $\mu\text{mol h}^{-1}$, respectively, this sample suffers from a poor photostability: its activity merely sustains in the first 2–3 h. In contrast, the Cu₂O@ZnCr-LDH nanospheres sample exhibits a stoichiometrical generation rate of 0.90 and 0.44 $\mu\text{mol h}^{-1}$ for H₂ and O₂, respectively, which is far superior to Cu₂O nanocubes. Moreover, the activity of Cu₂O@ZnCr-LDH photocatalyst maintains up to 5 h without any decline, demonstrating its rather high photostability. Taking into account the catalytic performance (evaluated by H₂ production rate), the Cu₂O@ZnCr-LDH sample is among the highest level for visible light water splitting compared with recently reported work (see details in the Supporting Information, Table S1). The apparent quantum

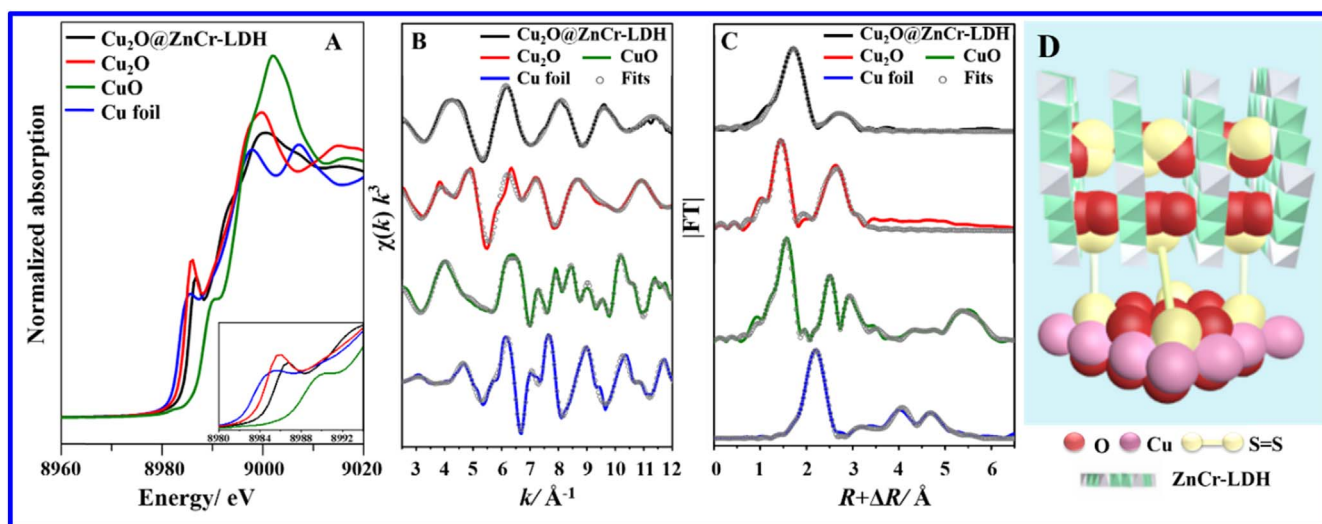


Fig. 4. Cu K-edge XAS data of Cu₂O@ZnCr-LDH and reference samples: Cu foil, Cu₂O and CuO. (A) Normalized XANES signals (inset: enlarged pre-edge region); (B) k^3 -weighted EXAFS oscillations; (C) Fourier transformed (not corrected for phase shift) EXAFS signals from k^3 -weighted oscillations. The solid line is experimental data and the grey dot is the fitting results; (D) schematic illustration for the interface of Cu₂O@ZnCr-LDH (S₂O₃²⁻ intercalated) structure.

Table 1
Local structure obtained from EXAFS refinement at Cu K-edge.^a

Sample	Atomic pair	CN	R (Å)	σ^2 (Å ² · 10 ³)	ΔE^0 (eV)	R factor %
Cu ₂ O@ZnCr-LDH	Cu–O	1.0(1)	1.95(2)	4.5(3)	–1.8(7)	0.44
	Cu–S	1.5(1)	2.22(1)			
	Cu–Cu	2.6(3)	3.09(1)	16.1 (1.3)		
Cu ₂ O	Cu–O	1.9(1)	1.85(1)	3.6(8)	–3.7(2)	2.34
	Cu–Cu	12.0(8)	3.03(1)	21.9 (1.7)		
	Cu–O	5.5(1.3)	3.56(1)	19.5 (9.8)		
CuO	Cu–O	3.9(1)	1.95(1)	4.5(3)	–0.4(1)	0.97
	Cu–Cu	3.9(2)	2.90(1)	6.1 (4)		
	Cu–Cu	3.9(2)	3.08(1)	7.9 (6)		
Cu	Cu–Cu	11.8(2)	2.54(1)	8.9(2)	–6.0(2)	1.10
	Cu–Cu	7.2(8)	3.58(1)	11.9 (1.7)		
	Cu–Cu	24.4(1.5)	4.45(1)	11.9 (8)		

^a CN: coordination number; R: atomic distance; σ^2 : Debye-Waller factor; ΔE^0 : shift of the threshold energy; R factor: goodness of fit. S_0^2 , 0.9358, was obtained from the experimental EXAFS fit of CuO by fixing CN as the known crystallographic parameter and was used for all the samples. Uncertainty is given by the number in bracket, i.e., 5.5(1.3) represents 5.5 ± 1.3 , and 3.03(1) means 3.03 ± 0.01 .

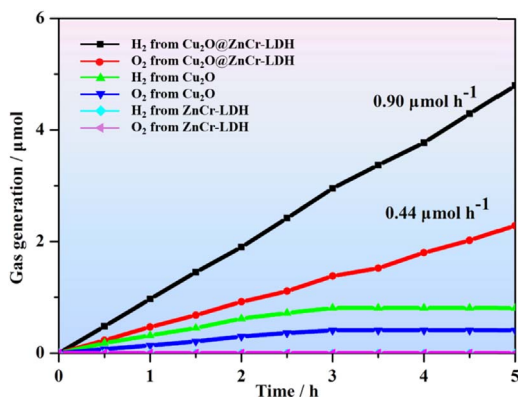


Fig. 5. Rate of gas generation as function of irradiation time ($\lambda > 400$ nm) within consecutive 5 h for ZnCr-LDH nanoplates, Cu₂O nanocubes and Cu₂O@ZnCr-LDH nanospheres, respectively.

efficiency (AQE) of Cu₂O@ZnCr-LDH photocatalyst is calculated to be ~0.2% (Supporting Information) in the visible light spectral range.

In addition, the XRD, SEM, TEM and EXAFS measurements (Fig. S7–S9) show no obvious change in its structure, coordination and morphology after 5 h photocatalytic reaction. The cycling tests for the visible-light-driven photocatalytic activity of Cu₂O@ZnCr-LDH nanospheres are illustrated in Fig. 6. Even after 5 consecutive runs without recovery of catalyst and reagent, the photocatalyst still maintains 90% of its original catalytic activity. The results demonstrate that Cu₂O@ZnCr-LDH core-shell nanospheres can serve as a promising photocatalyst for visible-light-induced overall water splitting with high activity and excellent recyclability.

3.4. Study on the structure-property correlation

To give a deep study on the crucial role of interlayer $S_2O_3^{2-}$ for the enhancement of Cu₂O@ZnCr-LDH photocatalyst, other two anions ($S_2O_8^{2-}$ and SO_4^{2-}) are respectively incorporated into the gallery of ZnCr-LDH during the synthesis process to give a comparison study (Fig. S10). When the interlayer anion is completely exchanged by

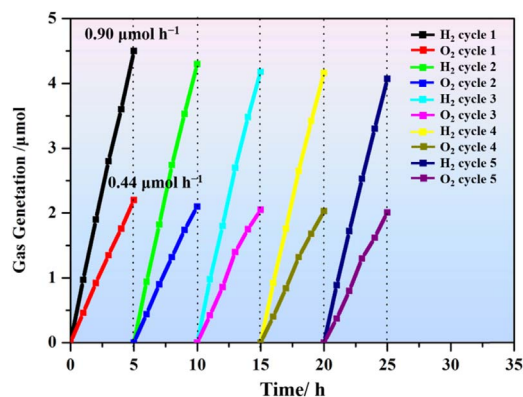


Fig. 6. Rate of gas generation as a function of irradiation time ($\lambda > 400$ nm) in 5 consecutive cycles (5 h/cycle) over Cu₂O@ZnCr-LDH photocatalyst.

$S_2O_8^{2-}$, no catalytic activity is observed. A partial substitution of interlayer $S_2O_3^{2-}$ by SO_4^{2-} induces an obvious decrease in the catalytic activity (Fig. S11). In addition to the Cu₂O@ZnCr-LDH sample, Zn(OH)₂ or Cr(OH)₃ nanoplate is also applied as shell material to construct core-shell heterostructure photocatalyst. The obtained Cu₂O@Zn(OH)₂ and Cu₂O@Cr(OH)₃ display a similar morphology (Fig. S12) with Cu₂O@ZnCr-LDH nanospheres, but exhibit no photocatalytic activity under the same conditions. Furthermore, elemental analysis results of Cu₂O@Zn(OH)₂ and Cu₂O@Cr(OH)₃ show that the mass fraction of Cu element is less than 0.1%. The result indicates that, without $S_2O_3^{2-}$ /LDH intercalated structure, Cu₂O nanocubes would be totally etched with the absence of interface interaction via Cu–($S_2O_3^{2-}$)/LDH bond. Therefore, the interlayer $S_2O_3^{2-}$ plays a key role in this Cu₂O@ZnCr-LDH photocatalyst: it maintains a structural integrity of the heterostructure by simultaneously interacting with positively-charged LDH host matrix and participating in the coordination with Cu₂O. This specific configuration of heterojunction, to the best of our knowledge, has not been reported so far.

To gain further insight into the electron-hole transport mechanism in the Cu₂O@ZnCr-LDH photocatalyst, density functional theory (DFT) calculations were carried out to elucidate the electronic structure of Cu₂O, ZnCr-LDH and Cu₂O@ZnCr-LDH from the theoretical viewpoint. The band edge placements of Cu₂O and ZnCr-LDH are calculated with Eqs. (1) and (2) [41,42]:

$$E_{CBM} = E_F + x = -W + x \quad (1)$$

$$E_{VBM} = E_{CBM} - E_g = -W + x - E_g \quad (2)$$

where E_{CBM} represents the energy level of conduction band minimum (CBM); E_{VBM} denotes the energy level of valence band maximum (VBM); E_g is the band gap energy; E_F is the energy level of Fermi level; W is the work function, and x is the energy difference between E_F and E_{CBM} . Based on the calculation results of band structure (Fig. S13), work function (Fig. S14) and molecular dynamics (MD) simulations at different time (Fig. 7A and B), the total density of states (TDOS) for Cu₂O and ZnCr-LDH are presented in Fig. 7C and D, respectively. The TDOS of Cu₂O is constituted by the Cu-3d and O-2p orbit and that of ZnCr-LDH is composed of the Zn-4s, Zn-4p, Zn-3d, Cr-3d and O-2p orbit. Since the VB of Cu₂O is lower than the CB of ZnCr-LDH in position, the photoexcited electrons from CB of ZnCr-LDH can inject into the VB of Cu₂O. This neutralizes the photogenerated holes of Cu₂O and thus inhibits its self-oxidization, giving rise to a largely enhanced photostability. The remaining holes in the VB of ZnCr-LDH, and electrons in the CB of Cu₂O, are involved in the oxidization and reduction of water to produce O₂ and H₂, respectively (Fig. 7E). In such a Z-scheme heterojunction, the separation/transport of photogenerated electron-hole pairs is effectively accelerated, accounting for the high activity toward visible-light-driven overall water splitting.

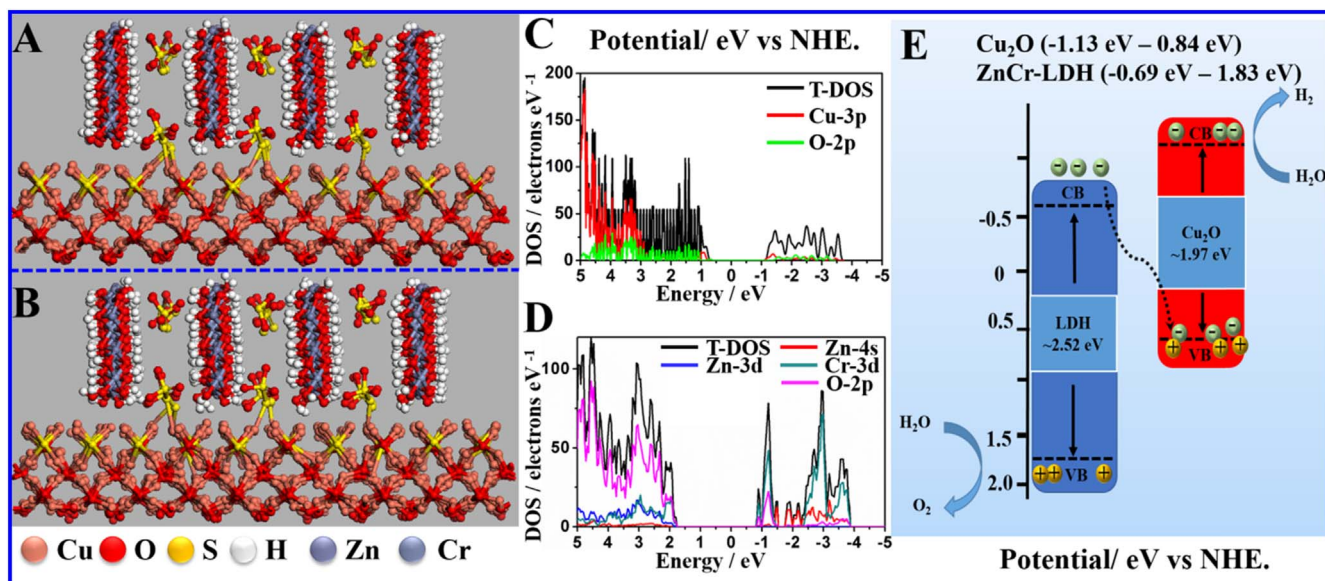


Fig. 7. Optimized geometry of molecular dynamics (MD) simulations for $\text{Cu}_2\text{O}@ZnCr\text{-LDH}$ ($\text{S}_2\text{O}_3^{2-}$ intercalated) model at (A) $t=50$ ps and (B) $t=100$ ps; the density of states for (C) Cu_2O and (D) $ZnCr\text{-LDH}$; (E) schematic illustration for the photoexcited electron separation/transport in the $\text{Cu}_2\text{O}@ZnCr\text{-LDH}$ system.

4. Conclusion

In summary, $\text{Cu}_2\text{O}@ZnCr\text{-LDH}$ with a core-shell heterostructure was fabricated by a facile in situ crystallization-selective etching method, which exhibits a high rate of H_2/O_2 generation and excellent photostability toward overall water splitting under visible light. The improved performance is attributed to the formation of $\text{Cu}-(\text{S}_2\text{O}_3^{2-})/\text{LDH}$ bond at the interface of $\text{Cu}_2\text{O}@ZnCr\text{-LDH}$ structure; $\text{S}_2\text{O}_3^{2-}$ maintains a structural integrity of the heterojunction by simultaneously interacting with positively-charged LDH host matrix and participating in the coordination with Cu_2O . DFT calculations reveal that the photoexcited electrons from CB of $ZnCr\text{-LDH}$ inject into the VB of Cu_2O , which promotes the electron-hole separation/transport and inhibits the self-oxidization of Cu_2O . This work provides a successful paradigm for the fabrication of Z-scheme heterojunction via band structure control and interfacial chemical tuning; it is expected that the strategy presented in this work can be extended to other semiconductor heterostructures for a variety of photocatalytic reactions.

Acknowledgment

This work was supported by the 973 Program (Grant No.: 2014CB932102) and the National Natural Science Foundation of China (Grant No.: 21671015 and U1407201) and the Beijing Nova program. We thank for the support of Beijing Synchrotron Radiation Facility (BSRF) on the XAFS measurements. We also appreciate kind help of Dr. Alejandro Fernandez-Martinez from Université Grenoble Alpes on the fitting of XAFS data.

Appendix A. Supporting information

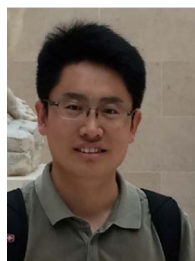
Supplementary data associated with this article can be found in the online version at [doi:10.1016/j.nanoen.2017.01.010](https://doi.org/10.1016/j.nanoen.2017.01.010).

References

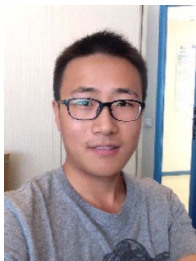
- [1] T. Takata, C. Pan, M. Nakabayashi, N. Shibata, K. Domen, *J. Am. Chem. Soc.* 137 (2015) 9627.
- [2] A. Fujishima, K. Honda, *Nature* 238 (1972) 37.
- [3] D. Kim, K.K. Sakimoto, D. Hong, P. Yang, *Angew. Chem. Int. Ed.* 54 (2015) 3259.
- [4] C. Cheng, W. Ren, H. Zhang, *Nano Energy* 5 (2014) 132.
- [5] G. Liu, J. Shi, F. Zhang, Z. Chen, J. Han, C. Ding, S. Chen, Z. Wang, H. Han, C. Li, *Angew. Chem. Int. Ed.* 53 (2014) 7295.
- [6] S. Ida, N. Kim, E. Ertekin, S. Takenaka, T. Ishihara, *J. Am. Chem. Soc.* 137 (2015) 239.
- [7] F. He, F. L. Energy *Environ. Sci.* 8 (2015) 535.
- [8] W.X. Guo, C. Xu, G. Zhu, C.F. Pan, C.J. Lin, Z.L. Wang, *Nano Energy* 1 (2012) 176.
- [9] X. Li, S. G. C. K. J. Zhu, T. Tong, S. Ke, W.C.H. Choy, B. Wei, *Nano Energy* 30 (2016) 549.
- [10] X. Zhang, Z. Lai, C. Tan, H. Zhang, *Angew. Chem. Int. Ed.* 55 (2016) 8816.
- [11] M. Li, L. Zhang, M. Wu, Y. Du, X. Fan, M. Wang, L. Zhang, Q. Kong, J. Shi, *Nano Energy* 19 (2016) 145.
- [12] H.M. Zhu, N. Song, T. Lian, *J. Am. Chem. Soc.* 133 (2011) 8762.
- [13] J. Hou, S. C. Y. Wu, F. Liang, L. Ye, Z. Lin, L. Sun, *Nano Energy* 30 (2016) 59.
- [14] L. Han, S. Dong, E. Wang, *Adv. Mater.* (2016). <http://dx.doi.org/10.1002/adma.201602270>.
- [15] H. Wu, H. Li, X. Zhao, Q. Liu, J. Wang, J. Xiao, S. Xie, R. Si, F. Yang, S. Miao, X. Guo, G. Wang, X. Bao, *Energy Environ. Sci.* (2016). <http://dx.doi.org/10.1039/c6ee01867j>.
- [16] R. Marschall, *Adv. Funct. Mater.* 24 (2014) 2421.
- [17] P. Zhou, J. Yu, M. Jaroniec, *Adv. Mater.* 26 (2014) 4920.
- [18] T. Wu, Q. Zhang, Y. Hou, L. Wang, C. Mao, S.-T. Zheng, X. Bu, P. Feng, *J. Am. Chem. Soc.* 135 (2013) 10250.
- [19] Y. Chen, S. Zhao, X. Wang, Q. Peng, R. Lin, Y. Wang, R. Shen, X. Cao, L. Zhang, G. Zhou, J. Li, A. Xia, Y. Li, *J. Am. Chem. Soc.* 138 (2016) 4286.
- [20] B. Ehrler, K.P. Musselman, M.L. Bohm, F.S.F. Morgenstern, Y. Vaynzof, B.J. Walker, J.L. MacManus-Driscoll, N.C. Greenham, *ACS Nano* 7 (2013) 4210.
- [21] L. Wang, J. Ge, A. Wang, M. Deng, X. Wang, S. Bai, R. Li, J. Jiang, Q. Zhang, Y. Luo, Y. Xiong, *Angew. Chem. Int. Ed.* 53 (2014) 5107.
- [22] A. Paracchino, V. Laporte, K. Sivula, M. Grätzel, E. Thimsen, *Nat. Mater.* 10 (2011) 456.
- [23] F. Li, L. Zhang, J. Tong, Y. Liu, S. Xu, Y. Cao, S. Cao, *Nano Energy* 27 (2016) 320.
- [24] X. Li, J. Yu, M. Jaroniec, *Chem. Soc. Rev.* 45 (2016) 2603.
- [25] M. Zhou, H.-L. Wang, S. Guo, *Chem. Soc. Rev.* 45 (2016) 1273.
- [26] D.B. Ingram, S. Linic, *J. Am. Chem. Soc.* 133 (2011) 5202.
- [27] Q. Wang, D. O'Hare, *Chem. Rev.* 112 (2012) 4124.
- [28] C. Li, M. Wei, D.G. Evans, X. Duan, *Small* 10 (2014) 4469.
- [29] J.L. Gunjekar, T.W. Kim, H.N. Kim, I.Y. Kim, S.-J. Hwang, *J. Am. Chem. Soc.* 133 (2011) 14998.
- [30] C.G. Silva, Y. Bouzvi, V. Fornés, H. García, *J. Am. Chem. Soc.* 131 (2009) 13833.
- [31] Y. Dou, S. Zhang, T. Pan, S. Xu, A. Zhou, M. Pu, H. Yan, J. Han, M. Wei, D.G. Evans, X. Duan, *Adv. Funct. Mater.* 25 (2015) 2243.
- [32] F. Ning, M. Shao, C. Zhang, S. Xu, M. Wei, X. Duan, *Nano Energy* 7 (2014) 134.
- [33] J. Nai, Y. Tian, X. Guan, L. Guo, *J. Am. Chem. Soc.* 135 (2013) 16082.
- [34] R.G. Pearson, *J. Am. Chem. Soc.* 85 (1963) 3533.
- [35] Z. Liu, R. Ma, Y. Ebina, N. Iyi, K. Takada, T. Sasaki, *Langmuir* 23 (2007) 861.
- [36] H.-L. Wu, R. Sato, A. Yamaguchi, M. Kimura, M. Haruta, H. Kurata, T. Teranishi, *Science* 351 (2016) 6279.
- [37] J. Nai, S. Wang, Y. Bai, L. Guo, *Small* 9 (2013) 3147.
- [38] Y. Fu, F. Ning, S. Xu, H. An, M. Shao, M. Wei, *J. Mater. Chem. A* 4 (2016) 3907.
- [39] R. Zhang, J.T. Miller, C.D. Baertsch, *J. Catal.* 294 (2012) 69.
- [40] H.-R. Jung, S.J. Cho, K.N. Kim, W.-J. Lee, *Electro. Acta* 56 (2011) 6722.
- [41] D.K. Kanan, E.A. Carter, *J. Phys. Chem. C* 116 (2012) 9876.
- [42] S.-M. Xu, T. Pan, Y.-B. Dou, H. Yan, S.-T. Zhang, F.-Y. Ning, W.-Y. Shi, M. Wei, *J. Phys. Chem. C* 119 (2015) 18823.



Chong Wang received his Bachelor's degree from Dalian University of Technology (DUT) in Applied Chemistry in 2011. He is now a Ph.D. candidate under the supervision of Prof. Min Wei in Beijing University of Chemical Technology (BUCT). His research is mainly focused on the heterostructure photocatalyst based on LDH materials.



Yufei Zhao is an associate professor at the Technical Institute of Physics and Chemistry, Chinese Academy of Sciences. He obtained his dual Bachelor's degrees in applied chemistry and computer science and technology at Shanxi University (2007), his Ph.D. degree in applied chemistry at Beijing University of Chemical Technology, under the supervision of Prof. Xue Duan and Prof. Min Wei in 2013. During 2011–2012, he visited University of Oxford as a joint Ph.D. student. His research focuses on layered double hydroxide based nanostructured photocatalysts for solar fuels.



Bin Ma received his Bachelor's degree from Dalian University of Technology (DUT) in 2011 and Master's degree from Peking University (PKU) in 2013, majoring in Applied Chemistry. He is now a 3rd year Ph.D. candidate, supervised by Prof. Laurent Charlet and Dr. Alejandro Fernandez-Martinez, at Université Grenoble Alpes (UGA, France). He specializes in immobilization of radionuclides (U, Se, Mo, etc.) in geological repositories for nuclear waste, and synchrotron-based X-ray techniques (XAS, PDF, SAXS, etc.).



Jingbin Han received his Ph.D. degree from Beijing University of Chemical Technology in 2011, after which he joined the staff of BUCT. He used to be a visiting student at the Georgia Institute of Technology (in 2009). He was also a visiting scholar at the University of Oxford (in 2014). His current interests are mainly focused on the design and fabrication of organic-inorganic functional materials and their applications in gas barrier and electrochemical energy storage.



Simin Xu received his Bachelor's degree from Beijing University of Chemical Technology (BUCT) in Applied Chemistry in 2011. He is now a Ph.D. candidate under the supervision of Prof. Xue Duan in the BUCT. His research interests mainly focus on the experimental and computational investigation of the physical and chemical properties of layered double hydroxides.



Min Wei obtained her BEng degree in 1995 and MEng degree in 1998 from Beijing University of Chemical Technology (BUCT). She subsequently received her Ph.D. from Peking University in 2001, after which she joined to the staff of BUCT. She was promoted to full Professor in 2005. She has been a visiting scholar in the Georgia Institute of Technology (in 2008). Her research interests focus on intercalation chemistry and functional materials as well as new catalysts.



Dapeng Li obtained his Bachelor's degree in 2014 from Zhengzhou University (ZZU). He is pursuing his master's degree under the guidance of Prof. Min Wei at the State Key Laboratory of Chemical Resource Engineering, Beijing University of Chemical Technology (BUCT). His research interests are the design and synthesis of LDH-based materials for visible-light-responsive photocatalysts.



David G. Evans studied as both an undergraduate and a research student at Jesus College, Oxford and obtained a DPhil under the supervision of Prof. D. M. P. Mingos FRS. After postdoctoral work at Bristol University with Prof. F. G. A. Stone FRS, he was appointed as a lecturer at Exeter University in 1985. He moved to Beijing University of Chemical Technology in 1996 and his research interests focus on intercalation in layered solids. He was awarded an International Scientific and Technological Cooperation Award of the People's Republic of China in 2005.



Shan He received his Ph.D. (2013) degrees from Beijing University of Chemical Technology, where he mainly studied on designing new catalysts based on layered double hydroxides under the supervision of Professor Xue Duan. In 2013, He continued working at Beijing University of Chemical Technology. His research interests focus on designing new catalytic materials and environmentally friendly catalysis.



Xue Duan was elected as an Academician of the Chinese Academy of Sciences in 2007. He was awarded his B.S. degree from Jilin University and M.S. and Ph.D. degrees from Beijing University of Chemical Technology (BUCT). He was subsequently appointed to the staff of BUCT and established the Applied Chemistry Research Institute in 1990. He was promoted to full professor in 1993 and to Ph.D. supervisor status in 1995. He is currently the director of the institute of Applied Chemistry and Executive Vice-Chair of the Academic Committee of the State Key Laboratory of Chemical Resource Engineering.